Microfluid Nanofluid (2008) 5:469–478
DOI 10.1007/s10404-007-0248-2

RESEARCH PAPER

Adherence and bouncing of liquid droplets impacting on dry surfaces

D. Caviezel · C. Narayanan · D. Lakehal

Received: 7 August 2007 / Accepted: 26 November 2007 / Published online: 25 January 2008

Abstract The paper explores liquid drop dynamics over a solid surface, focusing on adherence and bouncing phenomena. The study relies on detailed interface tracking simulations using the Level Set approach incorporated within a Navier–Stokes solver. The investigation deals with moderate Reynolds number droplet flows, for which two-dimensional axisymmetric simulations can be performed. The modelling approach has been validated against experiments for axisymmetric and full three-dimensional impact upon dry surfaces. A drop-impact regime map is generated for axisymmetric conditions, in which the impact dynamics is characterized as a function of Weber number and equilibrium contact angle, based on about 60 simulations. The detailed simulations also helped validate a new mechanistic model based on energy-balance analysis, delimiting the boundary between adherence and bouncing zones at low Weber numbers. The mechanistic model is only valid for moderate droplet Reynolds numbers and it complements existing models for higher Reynolds numbers.

List of symbols

g_i	gravity
u_i	velocity vector
a^{lg}	liquid–gas area
a^{sl}	solid–liquid area
A^{lg}	liquid–gas area
d	re-distance function
n_i	surface normal vector
s_i	surface tension
V	droplet volume
R	droplet radius
Re	Reynolds number
We	Weber number

Greek letters

η	viscosity
ρ	density
κ	surface curvature
γ	surface tension coefficient
σ	viscous stress
θ	equilibrium contact angle
δ^I	interface Dirac delta function
ϕ	Level Set
τ	pseudo time

Subscripts

lg	liquid–gas
ls	liquid–solid
sg	solid–gas

1 Introduction

Drop impact dynamics is important in a large application range, including ink-jet printing, rapid spray cooling of hot surfaces, direct jet impingement for power electronics cooling, quenching, etc. An unsuspected area of application is in petrochemical engineering, where the knowledge of the bouncing, spreading, and splashing characteristics of hydrocarbon oil drops is important for process engineering, and fuel characterization. Early studies of the impact process were more phenomenological in nature, looking mainly at the parameters influencing the spreading of the

D. Caviezel · C. Narayanan · D. Lakehal (✉)
ASCOMP GmbH, Technoparkstrasse 1,
8005 Zurich, Switzerland
e-mail: lakehal@ascomp.ch

D. Caviezel
e-mail: caviezel@ascomp.ch

liquid film on the surface. More recent studies (e.g., Rioboo et al. 2002) attempt to quantify the influence of individual parameters in order to obtain predictive capabilities of the impact process. The physics of drop impact on surfaces is multifaceted: a drop may be spherical or elliptic due to oscillations at the time of impact. The impact may be normal or oblique and the solid surface may be hard or soft, smooth or rough. But more importantly, the surface may be hydrophilic or hydrophobic, in which case the drop may bounce, spread or splash as a function of the dynamic contact angle at the three-phase junction.

Studying the limit separating droplet bouncing and non-bouncing regimes has importance in various applications. But most of the published contributions seem to deal with droplets colliding with gas–liquid interfaces rather than with solid walls. Bach et al. (2004) measured the trajectories of 20 and 40 μm radius water droplets colliding with a gas-water interface and determined the conditions under which drops bounce or coalesce. Drops were observed to undergo a transition from coalescence to bouncing as the Weber number is increased. They have also determined the apparent coefficient of restitution of the drops that bounce, which was found to decrease with increasing Weber number and becomes insensitive to the viscosity of the gas at Weber numbers larger than about unity. Another interesting study by Hsiao et al. (1998) focused on the critical Weber number for vortex and jet formation for drops impinging on a liquid pool. The importance of viscosity and impact velocity has been demonstrated by Mao et al. (1997) in their study of spread and rebound of droplets upon flat surfaces. The authors showed that increasing viscosity changes bouncing behavior to adherence, while increasing the impact velocity changes adherence to partial bouncing. Gilet et al. (2007) investigated experimentally the partial coalescence of a droplet onto a planar liquid–liquid interface by tuning the viscosities of both liquids. They found the problem to mainly depend on four dimensionless parameters: The Bond number, the Ohnesorge numbers in both fluids, and the density difference. On the computational front, we can cite the contribution of Nikolopoulos et al. (2007), who simulated in three dimensions a droplet impinging normally onto a wall film, and identified the mechanisms leading to secondary droplet formation. Various other similar simulations (in 2D and 3D) can be found in the literature, e.g., (Bussmann et al. 2000; Renardy et al. 2003). In these simulations, the focus was on describing the mechanisms of toroid formation and breakup.

In this paper we explore in detail liquid droplet adherence and bouncing phenomena for moderate Reynolds numbers, using computational multi-fluid dynamics (CMFD). The first main goal is to determine the limit separating adherence and bouncing of liquid drops impacting dry, smooth, and solid surfaces. For this purpose, we use the Level Set method (Sussman et al. 1994; Lakehal et al. 2002) for interface tracking implemented within a full Navier–Stokes solver, which we have first validated against experiments for axi-symmetric and full three-dimensional impact upon dry surfaces. The adherence and bouncing simulations were performed under axisymmetric conditions. Only non-wetting conditions have been considered, for which the equilibrium contact angle θ varies from 90° to 150°. The measurements of Rioboo et al. (2002) were used for validation. Fixing the Reynolds number ($Re = 800$), we ran about 60 simulations for different equilibrium contact angles and surface tension coefficients. The findings are compiled in the form of a new drop-impact regime map, in which the impact dynamics can be characterized as a function of Weber number and equilibrium contact angle. The next main objective is to propose a new mechanistic model based on energy-balance analysis, delimiting the drop-impact regime map into adherence and bouncing zones, valid for moderate droplet Reynolds numbers, complementing existing models for higher Reynolds numbers, e.g., (Mao et al. 1997).

2 Methodology

2.1 TransAT© micro-fluidics code

The CMFD code, TransAT (Transport phenomena Analysis Tool, http://www.ascomp.ch/transat.html), developed at ASCOMP is a multi-physics, finite-volume code based on solving multi-fluid Navier–Stokes equations. The code uses multi-block structured meshes, along with MPI based parallel capabilities. The grid arrangement is collocated and can handle curvilinear skewed grids. The solver is pressure based (projection type), using the Rhie–Chow correction to prevent pressure–velocity decoupling. High-order time marching and convection schemes can be employed; up to third order monotone schemes in space. For two-phase flow simulation, both the Level Set and the volume of fluid interface tracking methods can be used.

2.2 Transport equations

The incompressible fluid dynamics equations expressed within the one-fluid formalism take the following form,

$$\frac{\partial u_j}{\partial x_j} = 0 \tag{1}$$

$$\frac{\partial \rho u_i}{\partial t} + \frac{\partial (\rho u_i u_j)}{\partial x_j} - \frac{\partial \sigma_{ij}}{\partial x_j} = \rho g_i + s_i \tag{2}$$

where the RHS terms in the momentum equation (Eq. 2) represent gravity force, and the surface tension expressed

by Eq. (4) below, respectively. In Eqs. (1) and (2), where phase change is not accounted for, σ_{ij} is the Newtonian stress tensor.

In the Level Set method the interface between two fluids is represented by a continuous function ϕ, representing the distance to the interface that is positive on one side and negative on the other. This way, both fluids are identified, and the location of the physical interface is associated with the zero level. The Level Set evolution equation is given by

$$\frac{\partial \phi}{\partial t} + u_j \frac{\partial \phi}{\partial x_j} = 0 \tag{3}$$

Material properties such as the density and viscosity are smoothed across the interface using a modified Heaviside function based on ϕ. Further, the fact that ϕ is a continuous function across the interface helps the accurate determination of the normal vector n_i to the interface, and thereby the surface curvature required for the definition of the surface tension,

$$s_i = \gamma \kappa n_i \delta^I(\phi) \tag{4}$$

where γ is the surface tension of the fluid pair, κ is the interfacial curvature, and δ^I is a smoothed Dirac delta function centered at the interface. The Level Set function ceases to be a signed distance from the interface after a single advection step of Eq. (3). To restore its correct distribution near the interface, a re-distancing problem is solved, in which the equation below is integrated to steady state:

$$\begin{gathered} \frac{\partial d}{\partial \tau} - sgn(d_0)(1 - |\nabla d|) = 0 \\ d_0(\mathbf{x}, \tau = 0) = \phi(\mathbf{x}, t) \end{gathered} \tag{5}$$

where $sgn(x)$ is the Signum function.

The contact angle has been fixed to the equilibrium contact angle in this study. This is done at every time step through the application of the 0 value of the level-set function at the wall. This simple approach could have problems because the level-set function is not smooth near the wall resulting in inaccuracies in the calculation of interface curvature. A remedial measure is presented by Lesage et al. (2007), where a different reinitialization method near the wall is proposed (we thank the reviewer for bringing this work to our attention). However, as our validation attempts show, this simple method is able to capture the transient dynamics of drop impact with acceptable fidelity.

2.3 Numerical details

The Navier–Stokes equations and the Level Set advection equation are solved using the third order Runge–Kutta explicit scheme for time integration. The convective fluxes are discretized using the third order QUICK scheme bounded using a TVD limiter. The diffusive fluxes are discretized using the second order central scheme. Mass conservation is a crucial issue in CMFD simulations using Level Set for interface tracking. These simulations suffer from gain or loss of mass if no further measures are taken. Details about alleviating the mass conservation issue in the approach can be found in Takahira et al. (2004). In TransAT, the Level Set re-distancing problem (Eq. 5) is solved after each Level Set advection step (Eq. 3) using the non-oscillatory (WENO) third order scheme.

2.4 Simulation set-up

The simulations have been performed under two-dimensional axisymmetric conditions, with orthogonal grids of size 75 × 60 cells for the coarse mesh simulations, and 160 × 120 cells for the refined mesh simulations. Simulations with the refined grid were performed for the cases where dry-out in the drop center occured if coarse grids were employed. With the Level Set, the user has to take care that small flow features like thin liquid layers are well resolved to prevent artificial breaking. The contact angle at the wall has been set as an equilibrium contact angle.

For all simulations presented in the map in Fig. 4, the same initial data have been employed, in particular the droplet Reynolds number ($Re = 800$), except for surface tension γ and equilibrium contact angle θ. The properties of the liquid and gas phases are:

- liquid phase: $\rho_l = 1{,}000$ kg/m^3; $\eta_l = 0.001$ kg/(m s); drop diameter, $D_0 = 2$ mm; initial drop velocity, $V_0 = 0.4$ m/s; initial distance from the drop center to the wall, $h_0 = 1.5$ mm.
- gas phase: $\rho_g = 1.205$ kg/m^3; $\eta_g = 0.1511 \times 10^{-4}$ kg/(m s).

2.5 Validation

2.5.1 Axisymmetric impact

In this section we consider the capability of TransAT in predicting axisymmetric drop impact over smooth surfaces. The experimental data selected for comparison are those published by Rioboo et al. (2002), a study that has dealt with the effect of varying fluid properties, Reynolds number and surface roughness. The contact angle in the experiment varied between $\theta_{adv} = 105°$ when the drop spread out, and $\theta_{rec} = 95°$ while receding.

Figure 1 shows various simulation sequences of the impact of a water drop ($\rho = 1{,}000$ kg/m^3, $\eta = 0.001$ kg/(m s)) with initial velocity $V_0 = 1.18$ m/s and diameter $D_0 = 2.75$ mm. The drop impacts on a non-wetting surface with a selected average contact angle $\theta = 100°$. The fluid surface tension coefficient is $\gamma = 0.075$ N/m. The figure compares the simulations to the experiment of Rioboo et al. (2002), where the water drop impacts on a wax surface. The axisymmetric simulation was performed on a 320 × 122 grid.

The result of the simulation agrees fairly well with the experiment, reproducing most of the details of the drop impact. The regime of partial bouncing is the key feature of this test case and this is reproduced in the simulation. After spreading and contracting, the liquid drop splits into two or more drops. If one of these drops adheres to the wall while the other(s) is thrown away in the axial direction, this behavior is called partial bouncing. The very last sequences in the figure reflect the capability of the code to model the pinching of the cone formed during partial bouncing. The simulation in question will not appear in the droplet-impact map to be discussed next, mainly because the Reynolds number here exceeds the range considered in the flow regime map study.

For these simulations, a slight gain in mass in the liquid phase has been noticed, which occurred mainly during the contraction phase of the drop and while a cylindrical shape forms in the center.

2.5.2 *Three-dimensional impact*

Further to the above validation for axisymmetric impact, we address here the predictive capability of TransAT for three-dimensional drop impact over smooth surfaces. The experimental data selected for comparison are also those of Rioboo et al. (2002), in which the contact angle varied between $\theta_{adv} = 105°$ when the drop spread out, and $\theta_{rec} = 95°$ while receding.

Figure 2 compares various simulated impact sequences of a water drop on a wax surface to the experiment of Rioboo et al. (2002). The physical parameters taken are: $\rho = 1{,}000$ kg/m^3, $\eta = 0.001$ kg/(m s) with initial velocity $V_0 = 3.6$ m/s and diameter $D_0 = 3.17$ mm. The drop impacts on a non-wetting surface with a selected contact angle $\theta = 100°$, where the surface tension coefficient is $\gamma = 0.075$ N/m. The 3D simulation was performed on a 200 × 200 × 80 grid, distributed in parallel over 16 CPUs using MPI. The simulation took around 60 h on a Linux cluster. The Level Set advection and reinitialisation in this case caused slightly more mass gain (still within acceptable limits) than in the previous two-dimensional simulation.

The computational results agree well with the experiment, reproducing most of the drop-impact details. The drop-impact regime considered here is hardly identifiable from the experimental visualizations, but tends to be closer to partial bounce. It could also be at the limit of bouncing. The re-wetting scenario of the drop together with the circumferential fingering is well reproduced. The number of satellite drops is about 17–19 in the experiment; CMFD predicts about 15–16. The final sequence in the impact process shows the simulations to predict satellite droplets with little velocity after pinch off, tending to remain where they are deposited. This result which is not clear from this experiment has been obtained by Bussmann et al. (2000), who compared the data to another experiment. Nonetheless, the comparison with the experiment is satisfactory; a more refined grid (or better, a local grid refinement) should provide a more detailed picture of the flow.

3 Results and discussion

3.1 Axisymmetric impact

Selected results from the simulations performed to create the map are shown in Fig. 3. The main sequences of the impact process shown in these figures refer to (1) droplet adherence occurring for contact angle of 118° and $We = 0.44$, (2) bouncing without torus formation for contact angle of 129° and $We = 0.44$, and (3) bouncing with torus formation for contact angle of 129° and $We = 20$.

To proceed further with the discussion of the droplet-impact regime map presented in Fig. 4, we first introduce the main flow features relating to the deformation, elongation, spreading and receding of impacting droplets over solid surfaces, as is conventionally denoted in the literature. The following definitions will be used:

- *Adherence* This applies to liquid droplets that cannot recover enough kinetic energy to rebound. The droplets have the tendency to stick to the surface, reaching equilibrium after several oscillations. An example of adherence is shown in Fig. 3 (left).
- *Bouncing without torus formation* Here the droplets recover enough kinetic energy to bounce back from the wall, with a similar shape to that they had before impacting the surface. In this case the rate of spreading at impact is relatively low as compared to the case of bouncing with torus formation discussed next. An example is shown in Fig. 3 (middle).
- *Bouncing with torus formation* If the drop forms a torus at maximum spread-out without any liquid in the

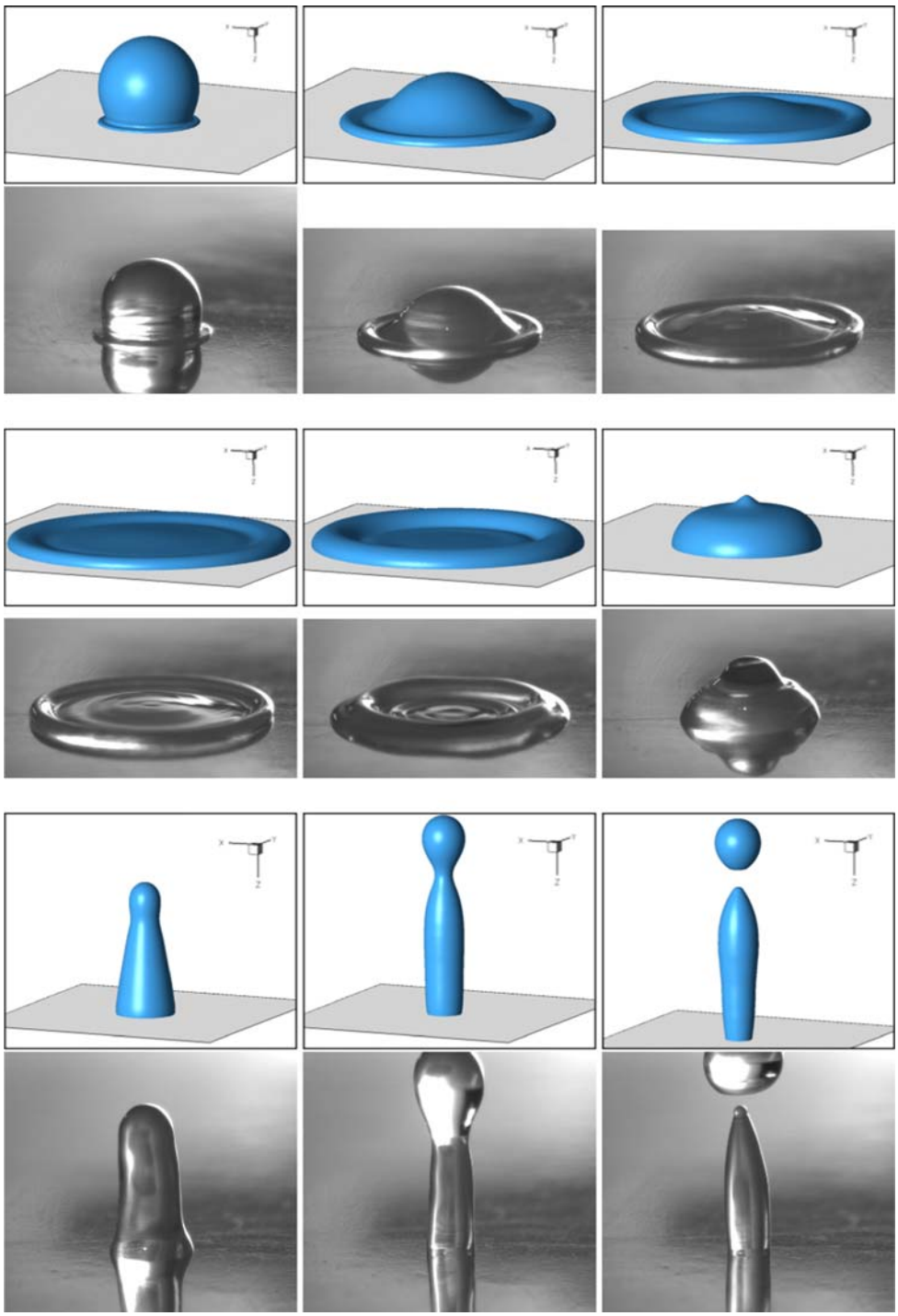

Fig. 1 Partial bouncing obtained for $\theta = 100°$, $We = 52$, $Re = 3{,}245$. Time history: experiment (simulation) in ms: $t = 0.45(0.32)$, 1.31(1.34), 2.25(2.26), 3.14(3.55), 6.02(5.96), 10.26(10.26), 14.02(13.96), 20.54(19.6), 25.58(23.14)

center, this is called dry-out. In an axisymmetric simulation, this torus will always contract back to form a drop. This may also happen in a three-dimensional simulation, but there could be circumferential instability effects that break the torus into fingers and wrinkles. The shrinking torus can breakup into a number of fingers, known as receding breakup (Yarin 2006). An example of bouncing with torus formation is shown in Fig. 3 (right).

- *Splashing* Splashing is a three-dimensional process, and can not be therefore reproduced properly by an axisymmetric simulation. Droplets can not be represented away from the rotation axis in axisymmetric simulations. Therefore, in this section, the droplet

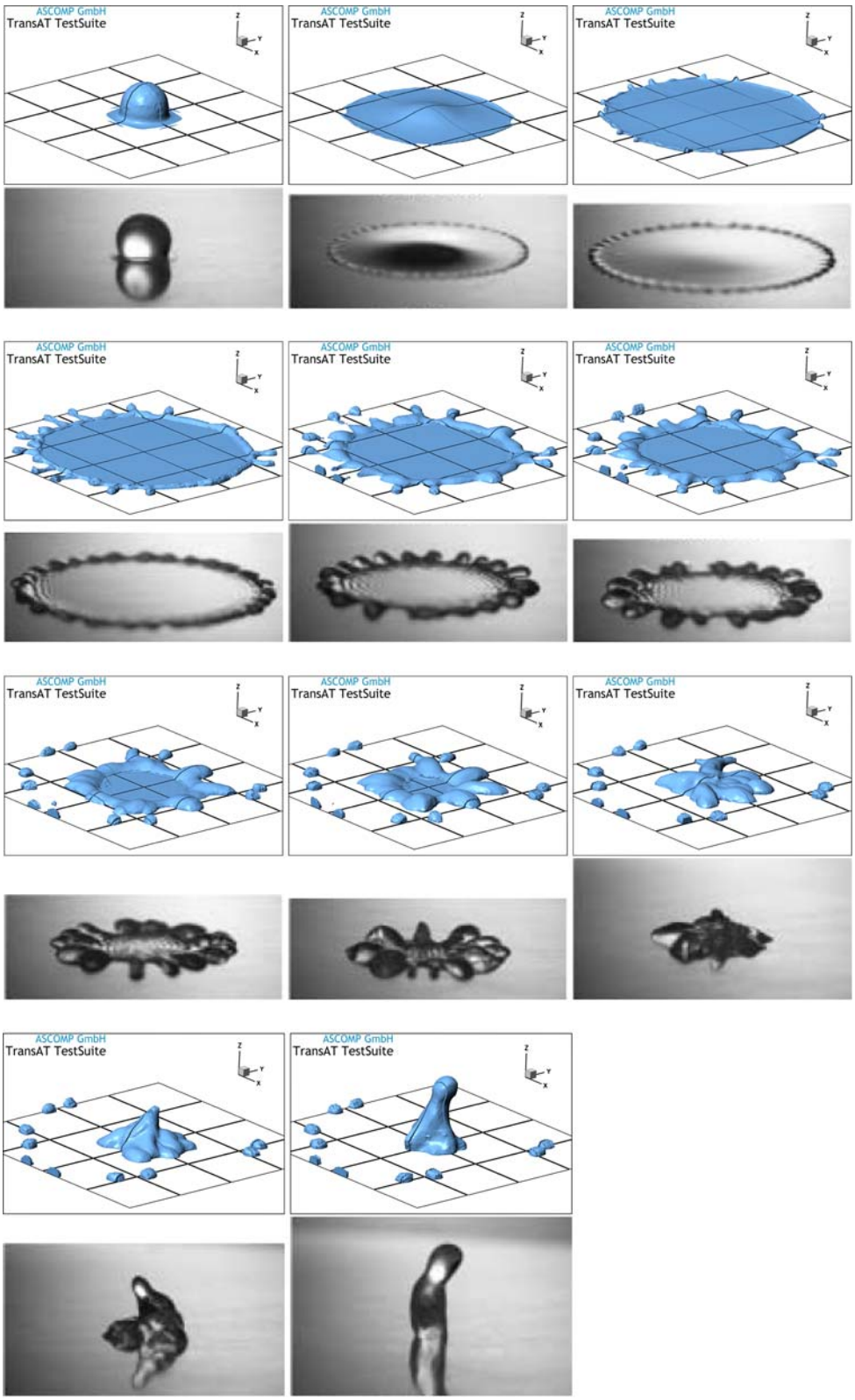

Fig. 2 Partial bouncing obtained for $\theta = 100°$, $We = 548$, $Re = 1{,}1412$. Time history: experiment (simulation) in ms: $t = 0.16(0.22)$, $1.02(1.2)$, $1.98(2.07)$, $4.42(4.43)$, $7.05(7.1)$, $7.94(8)$, $9.94(11.2)$, $11.19(12.8)$, $13.74(15.05)$, $15.06(16.5)$, $20.02(19.93)$

impact is called splashing if part of it is thrown away in the radial direction from the rest of the liquid core. The drop impact is also called splashing if the drop deformation is large during impact and the drop is not able to bounce, so that three-dimensional effects could split the drop into several droplets adhering to the wall.

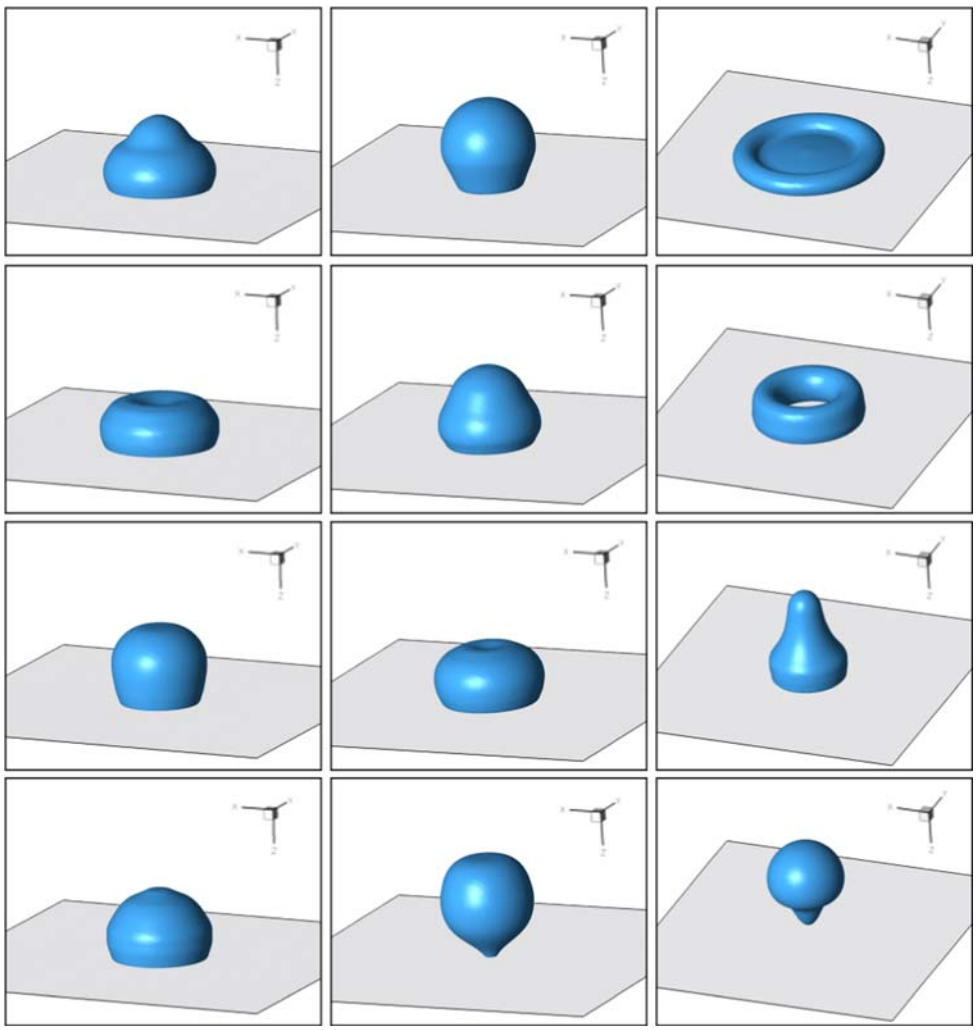

Fig. 3 *Left*: Adherence obtained for: $\theta = 118°$, $We = 0.44$. Time history in ms: $t = 2.5,3,4.5,8.3$. *Middle*: Bouncing without torus formation obtained for: $\theta = 129°$, $We = 0.44$. Time history in ms: $t = 1.6,2.2,2.8,6.7$. *Right*: bouncing with torus formation obtained for: $\theta = 129°$, $We = 20$. Time history in ms: $t = 7, 12.9, 18.5, 33$

3.2 Drop impact map

The simulation campaign undertaken in this work has led to the establishment of a droplet-impact regime map, in which the impact dynamics is characterized as a function of Weber number (We) and equilibrium contact angle (θ). The Weber number is a measure of the ratio of the kinetic energy and surface energy, defined as

$$We = \frac{\rho u^2 D_0}{\gamma} \tag{6}$$

where ρ is the fluid density, u is the impact velocity, D_0 is the drop diameter before impact and γ is the surface tension. The Reynolds number ($Re = \rho u D_0/\eta = 800$) is kept fixed for all simulations.

The resulting different behaviors of a water drop impacting a smooth, solid, non-wetting surface are summarized in the impact map shown in Fig. 4. The experimental data available in the literature do not fall in the range of Reynolds number considered here, i.e., for

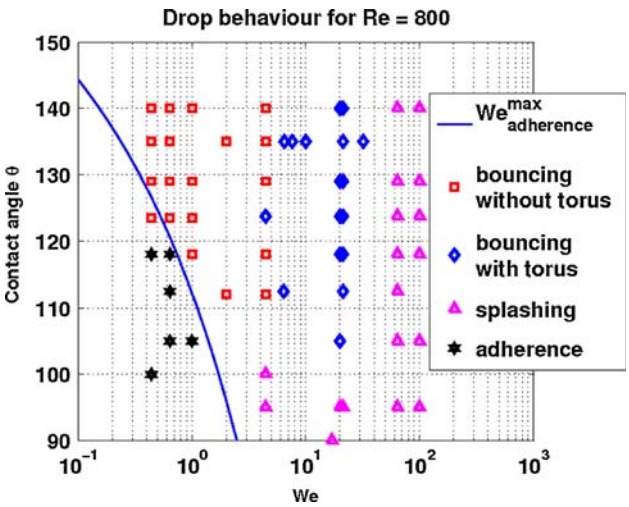

Fig. 4 Drop impact behavior map for Reynolds number $Re = 800$, depending on the Weber number and the equilibrium contact angle

which axisymmetric impact occurs. The map clearly depicts four different regimes:

- *Adherence* This has been obtained here for very small Weber numbers ($We \sim 0.1$) and low contact angles ($\theta < 120°$). The drop impact behavior is dominated by surface tension forces. The drop adheres to the wall, oscillating until reaching the equilibrium state.
- *Bouncing without torus formation* This has been obtained here for higher Weber numbers ($We \sim 1$), and higher contact angles ($\theta > 110°$), where surface tension effects are comparable to inertial effects. The shape of maximum deformation differs with surface tension values; for large values, the drop may deform weakly and rebound like a rubber ball. With decreasing surface tension, the drop spreads out at impact, creating a peripheral bulge connected by a liquid film in the center.
- *Bouncing with torus formation* This regime has been obtained for even higher Weber numbers ($We \sim 10$), and contact angles $\theta > 110°$. These conditions force the liquid film connecting the bulge at maximal deformation to rupture. Surface tension forces are still capable to contract the torus to a drop which then bounces.
- *Splashing* It is not easy to define splashing regime for axisymmetric simulations because the equilibrium state is always a drop adhering to the wall due to gravity. For high Weber numbers ($We \sim 100$), the drop breaks into several pieces moving in the radial direction away from the centerline. For lower Weber numbers (We $\sim$ 10) and low contact angles ($\theta < 100°$), strong deformations at drop impact can be observed, the drop spreading out to a diameter larger than four times the initial one, sometimes even breaks to several pieces. If the drop is not able to rebound, we call this impact behaviour also splashing.

The map also shows the influence of the equilibrium contact angle on the drop impact behavior. For low contact angles of 90°–95°, no complete bouncing drop could be simulated. The drop adheres to the wall or forms a splashing pattern as surface tension is reduced. As the contact angle is increased to 105°, bouncing after forming a torus can be observed at a Weber number of $We \sim 20$. This drop impact behavior at this specific Weber number does not change if the contact angle is further increased. For a contact angle of $\theta > 120°$, clean rebound of the full drop without forming a torus can be observed at low Weber numbers. Increasing the contact angle is reflected by a reduction of the minimum Weber number for which bouncing without forming a torus occurs. The line $We^{\max}_{\text{adherence}}$, defined in the next subsection using a simple model comparing equilibrium energies, provides a good

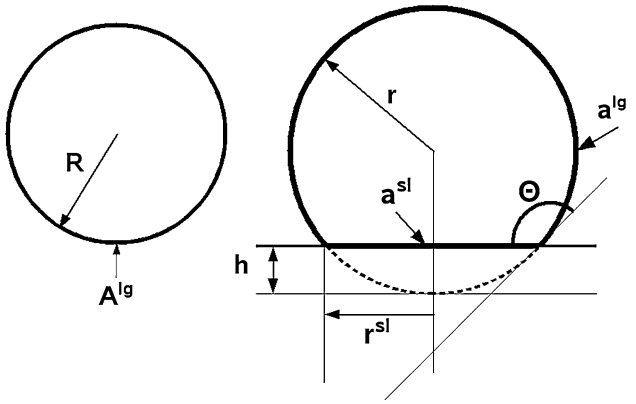

Fig. 5 Equilibrium shapes of a liquid drop surrounded by gas and a drop adhered to a wall, neglecting gravitational effects

estimation of the maximum Weber number for adherence. The splashing threshold as determined by our simulation is at around a critical Weber number of $W_c = 50$, which is slightly lower than the one observed by Wachters and Westerling (1966) ($W_c = 80$) for a number of different liquids impacting a polished gold surface. We also found splashing cases for lower Weber numbers and low contact angles $\theta < 100°$ according to our splashing definition. These cases should be further analyzed in three-dimensional simulations. We call this splashing because the drop deformation is high and the drop is not able to bounce. From the axisymmetric simulation we can not be sure the drop does not split into several droplets adhering to the wall.

The missing bouncing behavior in this map is partial bouncing, where the initial drop breaks after spreading and contraction into two or more drops; one staying at the wall with the others bouncing back. This pattern was not obtained probably because viscosity, impact velocity and thus the Reynolds number were kept constant for all simulations. The importance of viscosity and impact velocity has clearly been demonstrated in Mao et al. (1997). The authors show that increasing viscosity changes bouncing behavior to adherence, while increasing the impact velocity changes adherence to partial bouncing.

3.2.1 Mechanistic modeling

A simple estimation to determine the limit between adherence and bouncing regimes can be made by comparing the initial kinetic energy of the drop to the surface energy difference of a spherical drop at equilibrium, and a drop adhering to a wall, at equilibrium. The equilibrium state of a drop adhering to a wall has less total energy than a free drop at equilibrium having the same volume. For this

model, the two equilibrium energy states are compared neglecting gravity effects.

A perfect sphere with radius R, volume $V = \frac{4}{3}\pi R^3$, and surface $A = 4\pi R^2$ can be transformed in a cut sphere resting on a surface with volume (Fig. 5)

$$v = \frac{4}{3}\pi r^3 - \frac{1}{3}h^2\pi(3r - h) \tag{7}$$

where the height h of the missing spherical cap is defined by the contact angle θ by $h = r\ (1 - cos(\pi - \theta))$. By setting $V = v$ one can solve for the radius r of a spherical drop resting on a wall with contact angle θ having the same volume as a sphere with radius R (Rioboo et al. 2002):

$$r = 2R\left[2(1 - \cos\theta)(2 - \cos\theta - \cos^2\theta)\right]^{-1/3} \tag{8}$$

The total equilibrium energy of a free drop neglecting gravity consists of surface energy only, and is given by

$$E^0 = A^{\mathrm{lg}}\gamma_{\mathrm{lg}} = 4\pi R^2\gamma_{\mathrm{lg}} \tag{9}$$

where A^{lg}, γ_{lg} denote the liquid–gas interface area and liquid–gas surface tension. The equilibrium state of the drop adhering to the wall also consists only of surface energy, and is given by

$$\begin{aligned} E_w^0 &= a^{\mathrm{lg}}\gamma_{\mathrm{lg}} + a^{\mathrm{sl}}(\gamma_{\mathrm{sl}} - \gamma_{\mathrm{sg}}) \\ &= (4\pi r^2 - 2\pi rh)\gamma_{\mathrm{lg}} + \pi(r^{\mathrm{sl}})^2(\gamma_{\mathrm{sl}} - \gamma_{\mathrm{sg}}) \end{aligned} \tag{10}$$

where a^{lg}, a^{sl} denote the areas for the liquid–gas and solid-liquid interface, respectively. r^{sl} is the radius of the circular solid–liquid interface, defined by $r^{\mathrm{sl}} = r\sin(\pi - \theta)$. The solid–liquid and solid–gas surface tension difference $(\gamma_{\mathrm{sl}} - \gamma_{\mathrm{sg}})$ can be written as a function of the equilibrium contact angle θ and the liquid–gas surface tension γ_{lg} using Young's equation:

$$(\gamma_{\mathrm{sl}} - \gamma_{\mathrm{sg}}) = -\gamma_{\mathrm{lg}}\cos\theta \tag{11}$$

Substituting Eq. (11) into (10) and subtracting the result from Eq. (9), the energy difference of the two equilibrium states can be written as a surface area difference $\Delta A = \Delta A(\theta,R)$ which is only a function of the equilibrium contact angle θ, and the radius of the initial spherical drop R, times the liquid–gas surface tension:

$$\Delta E = \Delta A(\theta, R)\gamma_{\mathrm{lg}} \tag{12}$$

For small Weber numbers, the drop impact is dominated by surface tension effects. The drop immediately sticks to the wall and dissipates its energy by oscillations. This implies that the drop cannot bounce back because there is not enough kinetic energy left to create again a sphere. The assumption for this analytical estimation is the following: If the initial kinetic energy is smaller than the energy gained by adhering to the wall, $E_k^0 \le \Delta E = \Delta A(\theta,R)\gamma_{\mathrm{lg}}$, surface tension effects will help stick the drop to the wall.

Instead of writing a limit for the initial kinetic energy we can also write a limit for the Weber number. A drop with initial spherical shape of radius R should adhere if:

$$We_{\mathrm{adherence}} \le \frac{3\Delta A(\theta, R)}{\pi R^2}. \tag{13}$$

At least for the data we used in this investigation ($Re = 800$), the curve defined by the above expression (13) fits the simulation data quite well, as depicted in Fig. 4. Note that this model is only valid for low Weber numbers, when surface tension effects dominate inertia. For higher Weber and Reynolds numbers, inertia and viscosity play an important role too. A detailed model for higher Weber and Reynolds numbers also defining the adherence regime has been proposed by Mao et al. (1997), who also calculated energies, but also modeling the viscous dissipation, i.e., their model does not consider equilibrium states as in the present model. The viscous dissipation is modeled as an empirical correlation, using least-square data regression on experimental impact data. On the other hand their model is applicable only for impact velocities higher than 1 m/s, therefore it can not be compared to the present model. The two models can be thought of to complement each other, covering a wider range of droplet Reynolds numbers.

4 Conclusions

Drop impact behavior onto dry, smooth, non-wetting surfaces has been examined using simulations for variable Weber number and the equilibrium contact angle, where all other parameters had been fixed. Detailed interface tracking simulations using the Level Set approach have been performed for the purpose. The investigation deals with moderate Reynolds number droplet flows featuring axi-symmetric impact. A new drop-impact regime map has been proposed, in which the impact dynamics is characterised as a function of Weber number and equilibrium contact angle, based on the results of about 60 simulations. The detailed simulations also helped validate a new mechanistic model based on energy-equilibrium analysis, delimiting the drop-impact regime map into adherence and bouncing zones, valid for moderate droplet Reynolds numbers. The model was used to estimate and verify the adherence region in the impact map. The impact has been characterized by the ability of the droplets to bounce or not, and by the shape taken by the drop at maximum deformation. For the purpose of drawing the impact map, adherence, bouncing without torus formation and bouncing with torus formation have been successfully reproduced by the simulations.

The TransAT code has been validated for a problem involving partial bouncing (not present in the map); the

comparison with the experimental data was excellent. Future work will center around testing dynamic contact angle modeling rather than imposing an equilibrium contact angle. Also the influence of other non-dimensional numbers such as the Reynolds number have to be examined in order to extend the applicability of the map to more vigorous impacting conditions. This may explain why partial bouncing is missing in the proposed impact map.

Acknowledgements The authors are thankful to Dr R. Roberts (CHEVRON, USA) for the fruitful discussions on the subject.

References

Bach GA, Koch DL, Gopinath A (2004) Coalescence and bouncing of small aerosol droplets. J Fluid Mech 518:157

Bussmann M, Chandra S, Mostaghimi J (2000) Modeling the splash of a droplet impacting a solid surface. Phys Fluids 12:3121

Gilet T, Mulleners K, Lecomte JP, Vandewalle N, Dorbolo S (2007) Critical parameters for the partial coalescence of a droplet. Phys Rev E 75:036303

Hsiao M, Lichter S, Quintero L (1998) The critical Weber number for vortex and jet formation for drops impinging on a liquid pool. Phys Fluids 31:3560

Lakehal D, Meier M, Fulgosi M (2002) Interface tracking for the prediction of interfacial dynamics and heat/mass transfer in multiphase flows. Int J Heat Fluid Flow 23:242

Lesage A-C, Allain O, Dervieux A (2007) On level set modelling of bi-fluid flow. Int J Numer Meth Fluids 53:1297

Mao T, Kuhn DCS, Tran H (1997) Spread and rebound of liquid droplets upon impact on flat surfaces. AIChE J 43(9):2169

Nikolopoulos N, Theodorakakos A, Bergeles G (2007) Three-dimensional numerical investigation of a droplet impinging normally onto a wall film. J Comput Phys 225:322

Renardy Y, Popinet S et al (2003) Pyramidal and toroidal water drops after impact on a solid surface. J Fluid Mech 484:69

Rioboo R, Marengo M, Tropea C (2002) Time evolution of liquid drop impact onto solid, dry surfaces. Exp Fluids 33:112

Sussman M, Smereka S, Osher S (1994) A Levelset Approach for computing incompressible two-phase flow. J Comp Phys 114:146

Takahira H, Takahashi M, Banerjee S (2004) Numerical analysis of three-dimensional bubble growth and detachment in a shear flow. In: Proc. Int. Conf. Multiphase Flow (ICMF04), Yokohama, Japan, 30 May–04 June

Wachters LJH, Westerling NAJ (1966) The heat transfer from a hot wall to impinging water drops in the spheroidal state. Chem Eng Sci 21:1047

Yarin AL (2006) Drop Impact Dynamics: Splashing, Spreading, Receding, Bouncing. Annu Rev Fluid Mech 38:159